Investigation of Standing Waves on a String

Sayak Mukherjee, Blackett Laboratory, Imperial College London, London, SW7 2BB

***Abstract*—In this experiment, a guitar string attached to a sonometer was subjected to a tension of 4 N. The length of the string between the bridges of the sonometer was $0.69 \pm 0.02\,cm$. A detector was placed in the middle of the string and the string was plucked in the center just above the detector. This created an initial triangular displacement profile of the string which was allowed to oscillate after plucking. A sound-recording software called Audacity was used to record the string oscillations for approximately 20 seconds. The experimental data collected by Audacity was Fourier transformed using a FFT algorithm from Python. A super gaussian filter was used to discretely sample the frequencies of the string oscillations in frequency space. Seven harmonics were extracted from the data in total. Higher harmonics were ignored due to shorter lifetimes which did not produce enough data points to characterise them accurately. The decay constants of the harmonics were calculated. The even harmonics should not have existed due to the Fourier modes of the initial triangular profile. As a result, the even harmonics had faster decay constants than the odd harmonics because the even harmonics were unstable. The quality factor was calculated to be $Q = 520 \pm 14$ which showed that air resistance was not the main damping mechanism. A numerical simulation using finite difference schemes of second order in space and first order in time was made to solve the non-linear damping equation numerically. This showed that the even harmonics were created when the waves formed by the string were reflected from the ends of the sonometer. The waves reached the end of the sonometer because the bridge of the sonometer only simulated Dirichlet boundary conditions instead of Cauchy boundary conditions which resulted in waves passing through the bridge. A chi-squared test was conducted at the 1% significance level to determine how the linear approximation and the Dirichlet boundary conditions affected the data. It was found that the experimental data was accurate to $91.7 \pm 2.1\%$. This meant that the linear approximation and the Dirichlet boundary conditions were not good simplifications of the system. Other effects such as the stiffness of the string should be considered because air resistance was not the main damping effect as indicated by the high quality factor.**

I. Introduction

The history of waves dates back to the Ancient Greeks with Pythagoras investigating the relationship between sounds produced by the violin and the length of the strings needed to produce different harmonics. He developed the first mathematical relationship between frequency and waves derived from musical instruments [1]. Later on in the 17th century, it was Huygens who applied the idea of waves to the propagation of light. Hence, the famous Huygens' Principle was founded. This new theory of light propagation proved effective as the laws of reflection and refraction could now be proved analytically. Huygens' Principle was later verified by Young's double slit experiment [2]. Towards the latter part of the 17th century, using the recently discovered Newton's laws of motion, Brook Taylor derived the wave equation purely from intuition. By combining the wave equation and Joseph Fourier's work on expressing functions as an infinite summation of sinusoids, the connection between wave theory and Fourier theory became apparent. Much later in the 20th century, in the era of quantum mechanics, the concept of wave-particle duality first came to light when Albert Einstein suggested light is made of discrete energy packets called photons. Waves were then found in quantum mechanics through Schrodinger's equation and the standing waves in the famous infinite square well problem [3]. Since then, waves have been used in a myriad of applications ranging from electronics to signal processing. More recently, researchers have used gravitational waves as a method to confirm Einstein's General Theory of Relativity [4]. In this paper, we investigated standing waves on a string fixed at both ends and observed how the Fourier modes evolved. Finally, this was compared to a numerical simulation to understand how the approximations made affected the wave analysis.

II. Theory

The damped wave equation on a string is described by [5]:

$$\frac{\partial^2 u}{\partial t^2} = v^2 \frac{\partial^2 u}{\partial x^2} - C\hat{y}_t (\frac{\partial u}{\partial t})^2 \tag{1}$$

$u(x,t)$ represents the displacement of the string at position x at a time t. C is a constant related to the damping term and $\hat{y}_t$ represents the sign of the $\frac{\partial u}{\partial t}$ derivative. The $\hat{y}_t$ term ensures that the damping term acts opposite the displacement term. The damping of the string comes from the air resistance that the string encounters. However, this is a non-linear partial differential equation that cannot be solved analytically. Therefore, by making the assumption that the displacement of the string is small, the quadratic term becomes linear. Hence, the approximated equation becomes:

$$\frac{\partial^2 u}{\partial t^2} = v^2 \frac{\partial^2 u}{\partial x^2} - \gamma \frac{\partial u}{\partial t} \tag{2}$$

Here, the factor of $\hat{y}_t$ has been dropped because the $\frac{\partial u}{\partial t}$ term changes sign automatically. A new linear damping coefficient γ has been introduced instead of C. This equation is a linear equation which can be solved by separation of variables. By assuming $u(x,t) = X(x)T(t)$ and re-arranging the equation in the following manner [6]:

$$\frac{1}{T}\frac{d^2T}{dt^2} + \gamma \frac{1}{T}\frac{dT}{dt} = \frac{1}{X}\frac{d^2X}{dx^2} \tag{3}$$

The partial derivatives can be replaced by ordinary derivatives. As both sides of the equation depend on different independent variables they must be equal to a constant. Assuming the separation constant is $-k^2$ and solving the time and spatial equations separately:

$$\frac{d^2X}{dX^2} = -k^2X$$

$$\frac{d^2T}{dt^2} + \gamma\frac{dT}{dt} = -k^2T$$

The two ordinary differential equations above can be solved analytically. The total solution is then a superposition of both the solutions summed over all possible values of n.

$$u(x,t) = \Sigma_n\, A_n\, e^{-\frac{\gamma}{2}t}\, sin(\frac{n\pi x}{L})\, cos(\omega_n t) \tag{4}$$

The separation constant k is fixed by the spatial boundary conditions requiring $u(x = 0,\, t) = u(x = L,\, t) = 0$ which means $k = \frac{n\pi}{L}$ to ensure the sine term goes to 0 at the boundary. The temporal solution gives $\omega_n = \sqrt{(\frac{n\pi v}{L})^2 - (\frac{\gamma}{2})^2}$ where we have made the assumption that $\frac{\gamma}{2} << \frac{n\pi v}{L}$. The total solution then becomes a superposition of all the normal modes as indicated in equation 4.

A. Fourier modes of triangular function

After the string is plucked, the initial triangular wave would decompose into the normal modes derived in equation 4. A triangular function can be expressed as [7]

$$\text{u (x, t}_0) = \begin{cases} \frac{h}{p}x & 0 \le x \le p \\ \frac{h}{L-p}(L-x) & p \le x \le L \end{cases} \tag{5}$$

Here, t_0 indicates the time of the pluck. For this particular experiment $p = \frac{L}{2}$ as the string was plucked in the middle just above the detector.

The Fourier series of a function can be expressed as

$$f(x) = \frac{a_0}{2} + \sum_{n=1}^{\infty} a_n sin(nx) + b_n cos(nx)$$

The coefficients of the Fourier series a_n and b_n can be calculated by:

$$a_n = \frac{1}{2L}\int_0^L f(x) sin(nx) dx$$

$$b_n = \frac{1}{2L}\int_0^L f(x) cos(nx) dx$$

By using the integral definitions defined above, the Fourier series of the triangular function can be calculated for $p = \frac{L}{2}$ which yields:

$$u(x,t_0) = \begin{cases} \frac{8}{\pi^2 n^2}(-1)^{\frac{n-1}{2}} & odd\ n \\ 0 & even\ n \end{cases} \tag{6}$$

B. Numerical Simulation of PDE

A numerical simulation of equation 1 was created using finite difference schemes [8]. This was done to compare the approximations made for equation 2 to the original quadratic damped equation 1. The time derivatives and spatial derivatives can be characterised in the following manner:

$$\frac{\partial^2 u}{\partial t^2} = \frac{u^{n+1} - 2u^n + u^{n-1}}{\Delta t^2} + O(\Delta t^3) \tag{7}$$

$$\frac{\partial^2 u}{\partial x^2} = \frac{u_{j+1} - 2u_j + u_{j-1}}{\Delta x^2} + O(\Delta x^3) \tag{8}$$

$$(\frac{\partial u}{\partial t})^2 = \frac{(u^n - u^{n-1})^2}{\Delta t^2} + O(\Delta t^4) \tag{9}$$

To solve the whole equation an array of points can be created by assuming $n\Delta t = t$ and $j\Delta x = x$ where t and x represent the total time and total spatial range of the equation. Therefore, a grid of points can be constructed where u_j^n represents the n^{th} step in time and the j^{th} step in space. The grid of solutions would look as follows:

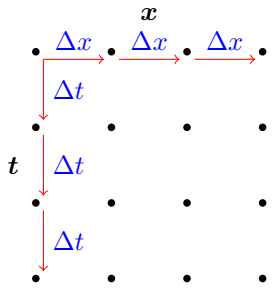

To propagate the solution in time, the finite difference schemes derived in equations 7, 8, 9 can be used to replace the derivatives in equation 1. This results in:

$$\frac{u_j^{n+1} - 2u_j^n + u_j^{n-1}}{\Delta t^2} = v^2\frac{u_{j+1}^n - 2u_j^n + u_{j-1}^n}{\Delta x^2} - C\hat{y}_t\frac{(u_j^n - u_j^{n-1})^2}{\Delta t^2}$$

This equation can be re-arranged to solve for u_j^{n+1} which yields:

$$u_j^{n+1} = 2u_j^n - u_j^{n-1} + \frac{v^2\Delta t^2}{\Delta x^2}(u_{j+1}^n - 2u_j^n + u_{j-1}^n) - C\hat{y}_t(u_j^n - u_j^{n-1})^2 \tag{10}$$

The initial condition of the wave was a triangular pulse and so the initial finite difference scheme required was $n = 0$. This reduces the equation to

$$u_j^1 = 2u_j^0 - u_j^{-1} + \frac{v^2\Delta t^2}{\Delta x^2}(u_{j+1}^0 - 2u_j^0 + u_{j-1}^0) - C\hat{y}_t(u_j^0 - u_j^{-1})^2 \tag{11}$$

The u_j^{-1} term can be solved for by setting the velocity of the string at $t = t_0$ to be 0. Hence, $\frac{\partial u}{\partial t} = 0$ meaning $\frac{u_j^{n+1} - u_j^{n-1}}{2\Delta x} = 0$ so $u_j^{n+1} = u_j^{n-1}$.

For the spatial part, Cauchy boundary conditions were applied to ensure that $u(x = 0, t) = u(x = L, t) = 0$

meaning $u_0^n = u_L^n = 0$ and $\frac{\partial u}{\partial x} = 0$ meaning $u_{-1}^n = u_1^n$ and $u_{L-1}^n = u_{L+1}^n$.

III. Experimental Setup

A sonometer was used to setup the experiment with a guitar string attached at both ends. The bridges of the sonometer were used to simulate fixed boundary conditions.

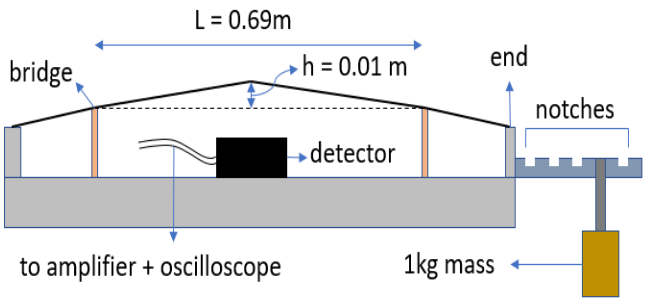

Fig. 1: This figure shows the guitar string attached to the sonometer. The string was fixed at both ends by the bridges on the sonometer. The detector was placed in the middle of the two bridges and connected to an amplifier and an oscilloscope. The string was plucked in the middle above the detector to a height h. This initially created a triangular displacement profile of the string. The lever arm with notches on the right side of the sonometer base adjusted the tension in the string. Each notch was a linear increase of the tension. For this experiment, a 1kg mass was placed on the fourth notch which meant the tension in the string was 4N.

After the string was plucked as shown in figure 1, the detector recorded the signal proportional to the velocity of the string. This signal was digitised by the amplifier. Finally, a sound-recording program called Audacity was used to record the digital signal from the amplifier. Care was taken to ensure that the string was not plucked with a large initial amplitude so that the string would have hit the detector. This was done to ensure that the string hitting the detector did not produce additional sound signals which the Audacity program might have interpreted as string vibrations.

A. Sources of Uncertainty

There were many sources of uncertainty in the experimental setup shown in figure 1. Firstly, the bridges that were used to simulate fixed boundary conditions for the string; only simulated Dirichlet boundary conditions instead of Cauchy boundary conditions. This meant that although $u(x = 0, t) = u(x = L, t) = 0$ was enforced, $\frac{\partial u}{\partial x} = 0$ at $x = 0$ and $x = L$ was not enforced by the bridges. As a result, some of the waves in the string could propagate through the bridges and get reflected by the ends of the sonometer. This lead to interference with the standing waves in the main experiment.

Secondly, the notches are spaced equidistant from one another to linearly increase the tension in the string. However, due to the design of the sonometer, there is a small spacing between the first notch and the edge of the sonometer meaning in the first notch there was some moment which induced some error in the tension.

Finally, there was the random error of positioning the bridges, the measurement of L, the measurement of h and the mass of the weights.

The random errors caused by the measurement of L and h from figure 1 and others were quantified by assigning a measurement error. These errors were propagated in quadrature to yield the final error on the string oscillation measurements. However, the reflection of waves from the ends of the sonometer was much harder to quantify. This is where the numerical simulation was used to quantify the error of these phenomena.

There were other smaller sources of error. For example, the linear damping term in equation 2 could be a function of pressure and temperature [9]. However, for this experiment this dependence was ignored as it was considered to be a small variation.

Another example, was the change in dimensions of the string as was put under tension. There was a volumetric change and the length of the string varied [10]. Once again, this was also ignored as the volumetric change for a guitar string of diameter $0.47 \pm 0.01\, mm$ was negligible.

IV. Results & Discussion

Once the data had been collected, Python was used to plot and analyse the data.

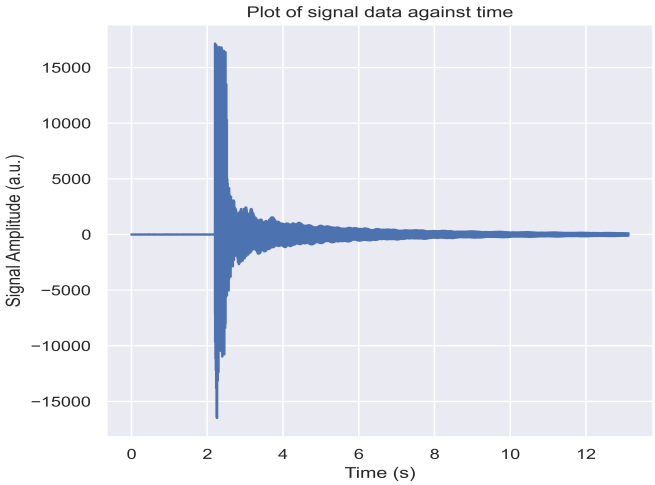

Fig. 2: This figure shows the signal recorded by the Audacity software against time. This graph provides a sanity check as it ensured that the data collection time was long enough to capture all of the oscillatory behaviour of the string. By looking at the decay profile of the signal it can be checked whether the gain of the amplifier was too high which would have resulted in the signal being saturated. In that case, a flat line would have been seen at the top before the decay of the signal.

The signal data was Fast-Fourier-Transformed (FFT) using the scipy package in Python. This was used to check the quality of the data.

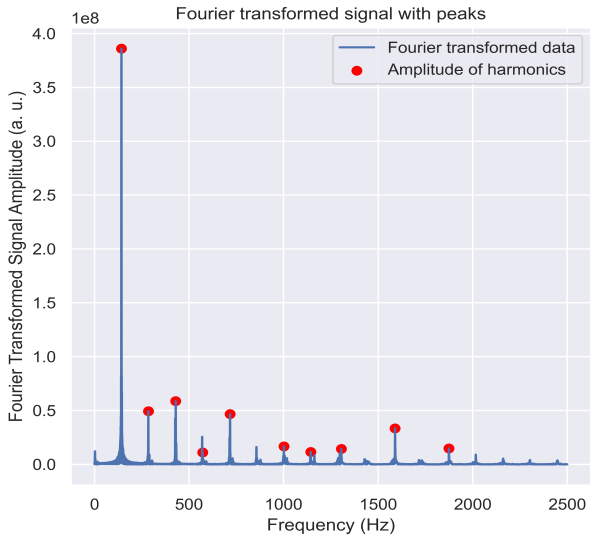

Fig. 3: This figure shows the Fourier transformed graph of the signal. The red dots indicate the peaks detected in the signal. The graph shows distinct peaks with relatively low noise. This means that the pluck height was sufficiently small such that the string did not hit the detector and generate unwanted harmonics. The pluck height was also sufficiently large to detect the Fourier modes present in the oscillation of the string.

The peaks were detected in figure 3 by using a peak detection package in scipy. A minimum threshold value of 1×10^7 was set to remove background noise whilst a constant distance between the peaks corresponding to the fundamental harmonic of around 142 Hz was used to detected the peaks.

A. *Filtering of data*

To extract the amplitude at each time, a filtering process was used. The filtering process could be applied either on the time space in figure 2 or the frequency space in figure 3. In this paper, the filtering process was applied to the frequency space because the frequency spectrum was discrete 1 which allowed for easier sampling.

As the string was plucked in the middle, $x = \frac{L}{2}$ was substituted into the normal modes derived in equation 4. Therefore, this gave an expression for the displacement of the string in the middle for each individual harmonic:

$$u(x = \frac{L}{2}, t) = A_n \, e^{-\frac{\gamma}{2}t} \, cos(\omega_n t) \tag{12}$$

By choosing each individual frequency from figure 3, and inverse Fourier transforming to time space, the analytic form of equation 12 was fitted to extract values of γ_n for different harmonics.

The most obvious choice for a filter would have been a top hat function [11] to sample the frequencies in frequency space. However, a product of functions in frequency space will become a convolution in time space when inverse Fourier transformed. The top hat function becomes a sinc function which is both positive and negative. Hence, this would have introduced errors into the data. So, a better choice of filter used was the super gaussian filter [12]. The Fourier transform of a gaussian function is still a gaussian so there are no instances where the filtering function goes negative. The reason for using a super gaussian filter was that it could effectively model sharp peaks better than a normal gaussian.

B. *Determining decay constants*

To determine the peaks from figure 3, thirty samples at equally spaced time intervals were chosen from figure 2. This temporal data was then Fourier transformed and the peaks located as shown in figure 3. Finally, a super gaussian filter was fitted around the peak of interest and then inverse Fourier transformed back to time space. The peaks from the oscillatory behaviour in the time space were extracted. Then, an exponential decay was fitted to this data to determine the decay constant for a particular harmonic. Thirty samples were chosen because if the super gaussian filter was too narrow in frequency space then they would become very wide in time space which would introduce errors. By trial and error, it was found that around thirty to forty samples gave best results.

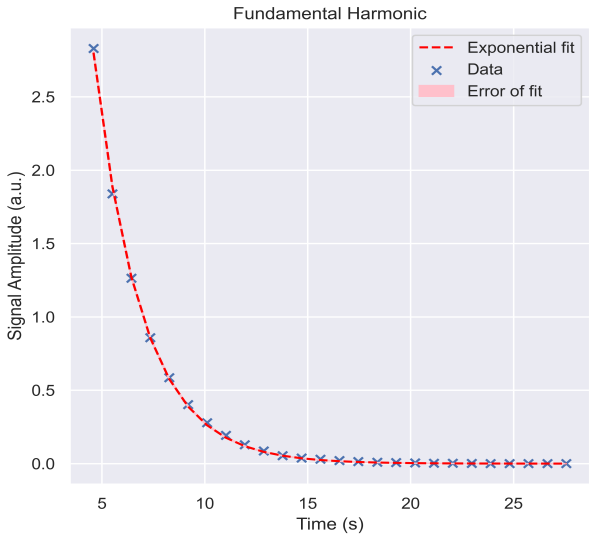

Fig. 4: This figure shows the decay of the fundamental harmonic with an exponential function fitted to the data. The fundamental harmonic corresponds to the peak with the largest amplitude in figure 3. The errors on the data points have been omitted because they were orders of magnitude smaller. The dominating source of error was the fit to the data.

The analysis can be repeated to find other harmonics by placing the super gaussian filter on the particular peak. Below is an example of the second harmonic.

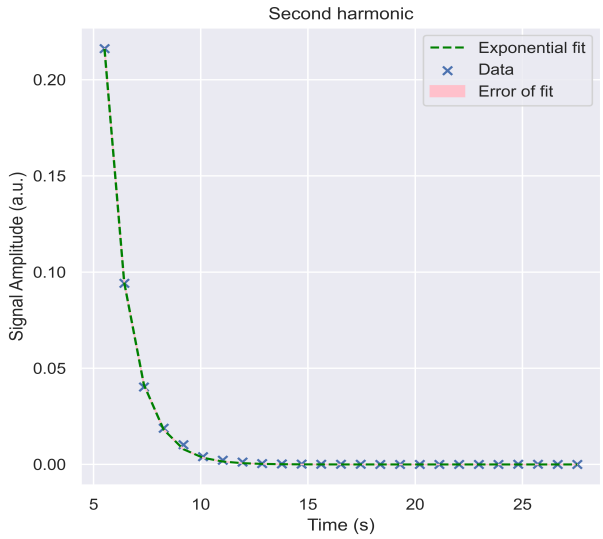

Fig. 5: This figure shows the decay for the second harmonic corresponding to the peak next to the fundamental harmonic in figure 3. By visually comparing the decay of the first and the second harmonic, it can be seen the second harmonic decays faster.

As the string was plucked like a triangular wave, the Fourier modes of this function which was derived in equation 6 contained no even harmonics. However, in the experimental data even harmonics do exist such as the one plotted above in figure 5. This means that the bridges of the sonometer in figure 1 simulated Dirichlet boundary conditions as discussed in section III-A. Therefore, the waves propagated through the bridges allowing the formation of even harmonics.

The decay constants upto the seventh harmonic was calculated. The higher harmonics were not calculated and simply ignored because their lifetimes were too short to obtain enough data points to accurately quantify them. Furthermore, the amplitudes of the higher harmonics were not distinct enough to separate them from the background noise.

Harmonic Number	Decay Constant (s^{-1})	Error (s^{-1})
1	0.86	0.01
2	1.85	0.10
3	0.81	0.02
4	1.55	0.06
5	1.19	0.01
6	2.06	0.03
7	1.58	0.06

TABLE I: This table is a summary of the decay constants upto the seventh harmonic. It is evident from the table that the even harmonics decayed much faster than the odd harmonics due to the instability of the even harmonics.

C. Determining the quality factor Q

The quality factor (Q) characterises whether the system is underdamped, overdamped or critically damped [13].

The quality factor can be determined by the equation:

$$Q = \frac{\omega_0}{2\gamma_n}$$

Here, ω_0 represents the fundamental angular frequency which is related to the fundamental frequency by $\omega_0 = 2\pi f_0$ with γ_n refering to the calculated decay constants determined above in table I. The quality factor was evaluated to $Q = 520 \pm 14$. As $Q >> 1$ that means the system was extremely underdamped and that air was not the main damping mechanism.

D. Comparison of experimental data to numerical simulation

The numerical simulation is the solution of equation 1. As this is a non-linear PDE, the Fourier modes derived in equation 4 will not be orthogonal to each other. Therefore, there will be some coupling effect between the modes [14]. Before comparing the experimental data to the numerical simulation, a sanity check of the simulation was required to ensure the simulation worked as intended.

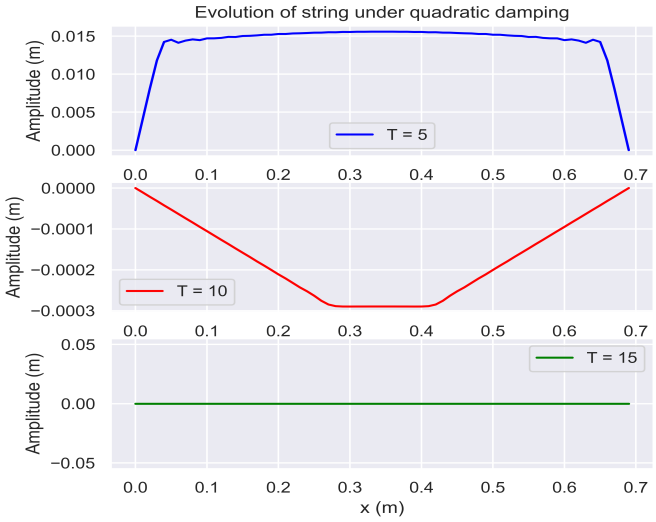

Fig. 6: This shows the evolution of the string at different points in time. By observing the $T = 5$ plot, it can be seen the triangular wave starts decomposing into modes that are out of phase with each other. However, at $T = 10$ they combine together to form a triangular wave. At $T = 15$ the string has stopped oscillating. The simulation was run with $\Delta x = 0.01$ and $\Delta t = 0.0001$ in relation to the finite difference scheme derived in equation 10. These plots provided a visual understanding to see if the simulation was working properly.

To further check the simulation worked properly, the quadratic damping constant (C) in equation 1 was set to 0. Therefore, a wave equation was simulated and this showed the simulation oscillated as pure Fourier modes without any decay. Then the quadratic damping was set to an arbitrarily

large number such as 1×10^5. This showed the simulation immediately returned to equilibrium without any oscillatory behaviour. These checks combined with figure 6 demonstrated the simulation worked as intended.

Finally, the simulation was compared to the experimental data where the value of the decay coefficient (C) was set to 1 to simulate typical values of air damping.

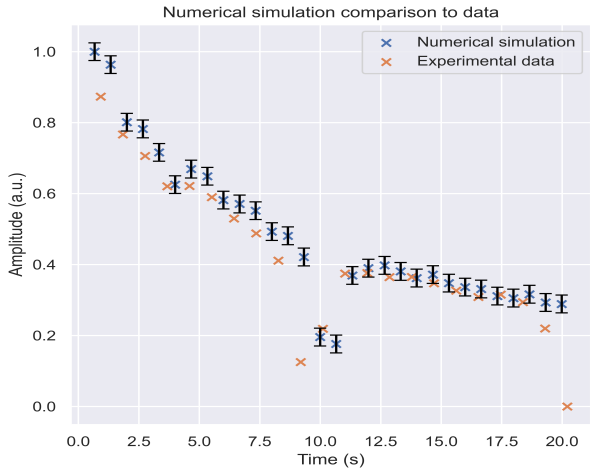

Fig. 7: This figure shows the comparison between the simulation and the actual data for the fundamental harmonic. The amplitudes of both the simulation and the experimental data was scaled to unity by integrating the area under the curve. A signal proportional to the velocity of the string at $x = \frac{L}{2}$ was extracted from the simulation. A similar filtering process as section IV-B was used to extract the decay constants. The error on the simulation was determined from the random uncertainty in L and h. The simulations were re-run with the L and h parameters changed and the difference was observed to calculate the error. The error propagation from the finite difference scheme was ignored because they were of order $O(\Delta x^2)$ and $\Delta x = 0.01$; so the random error dominated more than the numerical error. The experimental data was also shifted such that the pluck time t_0 corresponded to 0s.

The figure above shows the comparison for the fundamental harmonic. This process was repeated for the other harmonics. Even harmonics existed in the simulation as well, but they existed due to the coupling of modes arising from the quadratic diffusion term.

E. Chi-squared test of data

A chi-squared test was used to numerical quantify how much the linear approximation and the Dirichlet condition affected the data. The chi squared statistic was calculated using [15]:

$$\chi^2 = \sum \frac{(O-E)^2}{E}$$

Using the equation, the chi-squared statistic was evaluated for all of the seven harmonics.

Harmonic Number	χ^2	Error of χ^2
1	17.01	0.58
2	21.43	1.01
3	16.98	0.44
4	22.01	0.97
5	18,35	0.46
6	24.99	0.99
7	19.05	0.72

TABLE II: This table shows the χ^2 values of the harmonics. The even harmonics show a larger χ^2 value as expected. The errors on the χ^2 values were calculated from the error in figure 7 of the numerical simulation data points.

A hypothesis test was performed to check the accuracy of the experimental data.

H_0: **The linear approximation and the Dirichlet boundary conditions are good approximations.**

H_1: **The linear approximation and the Dirichlet boundary conditions are not good approximations.**

The mean of the χ^2 values from table II for all the harmonics was 19.97 ± 0.74. Therefore, $P(\chi^2) \leq 19.97 = 0.083$ at 30 degrees of freedom. As a result, there is sufficient evidence to reject H_0 at the 1% significance level. The experimental data is accurate to $91.7\% \pm 2.1\%$. Therefore, stiffness of the string and the reflection of waves from the Dirichlet boundary conditions affected the string oscillations.

V. Conclusion

Overall, the experiment demonstrated how the quadratic non-linear PDE for damped harmonic motion was approximated to a linear PDE. The analytical solution was compared to the experimental data by plucking the string generating an initial triangular displacement profile. The Fourier transform of this data using a super gaussian filter showed the harmonic content of the oscillating string. There were even harmonics which were not expected but arose from the Dirichlet boundary conditions imposed by the bridges and the coupling of modes due to the quadratic damping term. Finally, on comparison to the simulation of the non-linear PDE solution, it was determined that the experimental data was only accurate to $91.7 \pm 2.1\%$ meaning the Cauchy boundary conditions affected the data significantly. The main damping mechanism was not air because the quality factor of air damping was determined to be $Q = 520 \pm 14$. The main source of damping was the interference between standing waves and reflected waves from the edge of the sonometer and the stiffness of the string which is of the form $\kappa^2 \frac{\partial^4 u}{\partial x^4}$ [16]. To improve the experiment further, the gap between the detector and the string could be increased allowing the string to be plucked for greater amplitudes. Therefore, a boundary where the linear approximation breaks down can be identified. Furthermore, the simulation could be modified to include the stiffness term which enable us to determine to what extent the stiffness of the string affects the oscillatory behaviour. The experimental setup could be improved by having a Newton meter on the string to determine the precise tension in the guitar string.

REFERENCES

[1] A. Barker, "The science of harmonics in classical greece," 2007.

[2] B. B. Baker and E. T. Copson, *The mathematical theory of Huygens' principle*, vol. 329. American Mathematical Soc., 2003.

[3] J. G. Cramer, "The transactional interpretation of quantum mechanics," *Reviews of Modern Physics*, vol. 58, no. 3, p. 647, 1986.

[4] J. L. Cervantes-Cota, S. Galindo-Uribarri, and G. F. Smoot, "A brief history of gravitational waves," *Universe*, vol. 2, no. 3, p. 22, 2016.

[5] H. Laalej, Z. Q. Lang, S. Daley, I. Zazas, S. Billings, and G. Tomlinson, "Application of non-linear damping to vibration isolation: an experimental study," *Nonlinear Dynamics*, vol. 69, pp. 409–421, 2012.

[6] A. D. Polyanin and A. I. Zhurov, *Separation of variables and exact solutions to nonlinear PDEs*. CRC Press, 2021.

[7] Y. Wei, "Triangular function analysis," *Computers & Mathematics with Applications*, vol. 37, no. 6, pp. 37–56, 1999.

[8] J. C. Strikwerda, *Finite difference schemes and partial differential equations*. SIAM, 2004.

[9] A. Kiraci and H. Yurtseven, "Temperature dependence of the raman frequency, damping constant and the activation energy of a soft-optic mode in ferroelectric barium titanate," *Ferroelectrics*, vol. 432, no. 1, pp. 14–21, 2012.

[10] L. Gerward, "The bulk modulus and its pressure derivative for 18 metals," *Journal of Physics and Chemistry of Solids*, vol. 46, no. 8, pp. 925–927, 1985.

[11] B. Houshmand, W. C. Chew, and S.-W. Lee, "Fourier transform of a linear distribution with triangular support and its applications in electromagnetics," *IEEE transactions on antennas and propagation*, vol. 39, no. 2, pp. 252–254, 1991.

[12] D. Rativa and B. Vohnsen, "Single-and multimode characteristics of the foveal cones: the super-gaussian function," *Journal of Modern Optics*, vol. 58, no. 19-20, pp. 1809–1816, 2011.

[13] R. I. Parovik, "Quality factor of forced oscillations of a linear fractional oscillator," *Technical Physics*, vol. 65, pp. 1015–1019, 2020.

[14] A. I. Vistnes, *Physics of Oscillations and waves*. Springer, 2018.

[15] P. E. Greenwood and M. S. Nikulin, *A guide to chi-squared testing*, vol. 280. John Wiley & Sons, 1996.

[16] D.-h. Dan, Z.-h. Chen, and X.-f. Yan, "Closed-form formula of the transverse dynamic stiffness of a shallowly inclined taut cable," *Shock and Vibration*, vol. 2014, 2014.